Szalai, R., Tsaneva-Atanasova, K. T., Homer, M. E., Champneys, A. R., Kennedy, H. J., & Cooper, N. P. (2011). Nonlinear models of development, amplification and compression in the mammalian cochlea. 10.1098/rsta.2011.0192

Nonlinear models of development, amplification and compression in the mammalian cochlea

By R. Szalai, K. Tsaneva-Atanasova, M. E. Homer, A. R. Champneys †, H. J. Kennedy ‡, N. P. Cooper ¶

This paper reviews current understanding and presents new results on some of the nonlinear processes that underlie the function of the the mammalian cochlea. These processes occur within mechano-sensory hair cells that form part of the organ of Corti. After a general overview of cochlear physiology, mathematical modelling results are presented in three parts. First, the dynamic interplay between ion channels within the sensory *inner* hair cells is used to explain some new electrophysiological recordings from early development. Next, the state-of-the-art is reviewed in modelling the electro-motility present within the *outer* hair cells, including the current debate concerning the role of cell body motility versus active hair bundle dynamics. A simplified model is introduced that combines both effects in order to explain observed amplification and compression in experiments. Finally, new modelling evidence is presented that structural longitudinal coupling between outer hair cells may be necessary in order to capture all features of the observed mechanical responses.

Keywords: inner ear, inner hair cell, outer hair cell, compression, electromechanical transduction

1. Cochlear physiology

Hearing is a complex biological process, that relies on many highly developed subsystems. The main concern of this paper is the cochlea, which houses the first active and nonlinear components of the auditory system. The cochlea's most basic function is to convert sound-evoked motion into an ensemble of neural signals which underlies an organism's ability to hear.

A schematic view of the mammalian cochlea can be seen in Fig. 1(a,b). It is a coiled tube that consists of three fluid-filled chambers: the *scala tympani*, *scala media* and *scala vestibuli*. At the basal end there are two openings: the oval window, which is connected to the middle ear, and the round window, which is covered by an elastic membrane. The scala tympani and scala media are separated by the *organ of Corti*, which is built on the flexible *basilar membrane*. The scala media and scala tympani are separated only by the thin *Reissner's membrane* and are usually modelled as a single chamber.

† Department of Engineering Mathematics, University of Bristol, Bristol BS8 1TR, United Kingdom.

‡ School of Physiology and Pharmacology, University of Bristol, Bristol BS8 1TD, United Kingdom.

¶ School of Life Sciences, Keele University, Keele, Staffordshire ST5 5BG, United Kingdom.

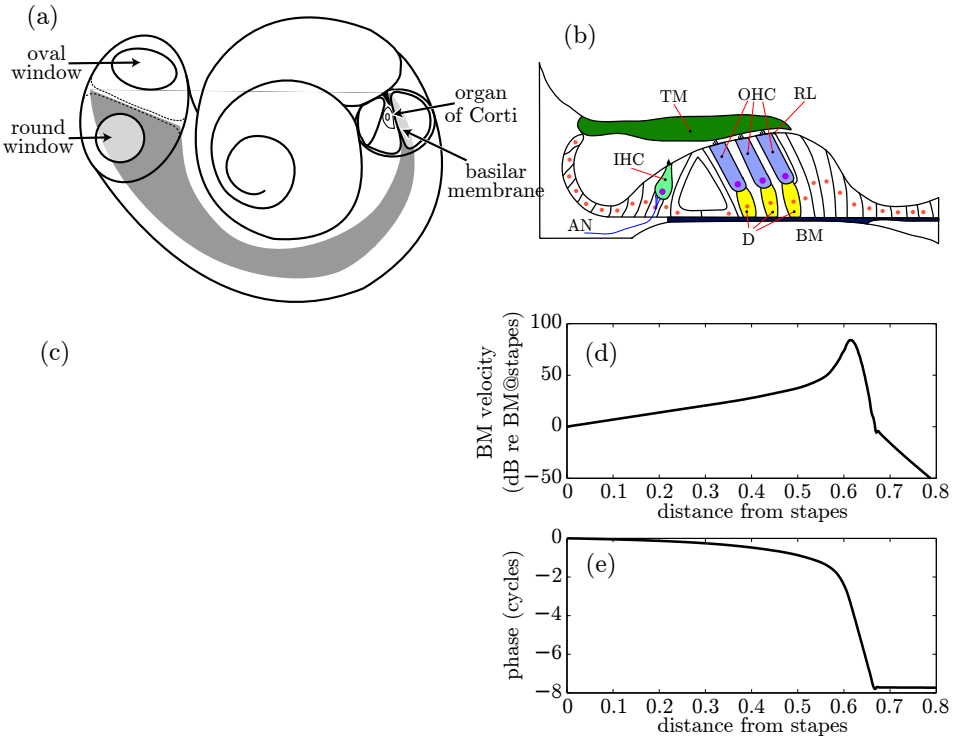

Figure 1. (a) A schematic view of the anatomy of the cochlea. (b) A schematic transverse section through the organ of Corti. Here TM represents the tectorial membrane, OHC an outer hair cell, RL the reticular lamina, BM the basilar membrane, D a Deiters' cell, AN an auditory nerve fibre and IHC an inner hair cell. (c) An image showing the arrangement of hair bundles of OHCs protruding beyond the RL in a view from above, with the vertical axis representing the radial direction and the horizontal axis representing the longitudinal direction. The image was downloaded from `http://www.udel.edu/biology/Wags/histopage/empage/ee/ee4.gif`. (d-e) Schematic representation of the amplitude and phase of a travelling wave with longitudinal distance along the basilar membrane.

A typical transverse cross-section through the organ of Corti is depicted schematically in Fig. 1(b); see also the photographic view from above in Fig. 1(c) with the tectorial membrane removed. The three rows of *outer hair cells* (OHCs) are connected to the basilar membrane by the *Deiters' cells*, and at the other end to the *reticular lamina*. The hair bundle of the OHCs are stimulated by the shearing motion of the *tectorial membrane* which slides above the reticular lamina as the basilar membrane is deflected by pressure differences between the fluid filled chambers. Sensing of sound occurs through the *inner hair cells* (IHCs), which are positioned on the opposite side of the *tunnel of Corti* (the triangular shaped void depicted in Fig. 1(b)). The inner hair cells signal the characteristics of a sound to the brain via synaptic contacts with individual fibres of the auditory nerve.

Attempts to understand the function of the human hearing organ can be traced to the work of Aristotle, who supposed that acoustic resonance occurs in an air filled

cavity located behind the eardrum; see Gitter (1990). The discovery of the anatomy of the basilar membrane by Hensen (1863) inspired Helmholtz (1863) to formulate the theory of tonotopy, also known as the place theory of hearing. Specifically, every transverse cross-section of the cochlea is most sensitive to a particular frequency, the so-called characteristic frequency (CF) of that location. The tonotopy map is such that low frequencies excite the basilar membrane at apical positions along the cochlear tube, while high frequencies stimulate the basal end. Helmholtz also recognised that merely having a resonant basilar membrane does not explain the observed sharp frequency discrimination. Therefore he hypothesised that there are additional oscillators connecting the basilar membrane and the sensory nerves.

The experiments of Békésy (1960) indicated that the fluid-structure interaction of the cochlear tube and membrane supports a travelling wave. This wave reaches a maximum amplitude and rapidly attenuates at a frequency-dependent distance from the stapes, thus explaining the tonotopic map. Such behaviour can be reproduced theoretically via a dynamic interplay between the fluid in the cochlear duct and the basilar membrane, with stiffness that varies with longitudinal position; see e.g. Zwislocki (1948), Lighthill (1981), and Lesser & Berkley (1972).

Békésy's experiments were conducted using high-amplitude stimulation of post-mortem cochleae, and revealed only relatively broadly tuned mechanics. Later experiments by Johnstone & Boyle (1967), Rhode (1971), and Sellick *et al.* (1982) found much sharper tuning and active mechanical responses in living animals. Another piece of evidence pointing to an active process in the cochlea's mechanics was the discovery by Kemp (1978) that sound is emitted from a healthy ear after a short stimulus, a phenomenon known as *otoacoustic emission*.

As experimental technology developed, it became possible to characterise the nonlinear vibrations of the active basilar membrane more fully (see Robles & Ruggero (2001) for review). Exemplar basilar membrane responses obtained by Rhode (2007) are shown in Fig. 4(b-c) for the 9.1 kHz CF position of the chinchilla cochlea when subjected to a range of different pure tone frequencies and amplitudes. These data represent the experimental results by which we shall benchmark modelling results in §3 and §4 below.

The active component of the cochlea's mechanics is widely accepted to be located within the OHCs of the organ of Corti. These particular cells have two types of active processes; see e.g. Dallos (2008) and Hudspeth (2008). The hair bundle on top of the cell is motile, and can hence exert force against the vibrating structures of the cochlea. For example, the experimental results of Kennedy *et al.* (2005) show that direct mechanical stimulation of the hair bundles can result in a period of negative stiffness. On the other hand it was observed by Brownell *et al.* (1985) that if OHCs are depolarised they shorten. Later Zheng *et al.* (2000) discovered that a piezoelectric protein called *prestin*, which is embedded within the lateral membrane of the OHC body is responsible for this effect. Prestin can expand and contract in response to changes in the cell potential, and makes the cell body change its shape. Both bundle motility and somatic motility can be stimulated by cochlear vibrations through the mechanically sensitive ion channels (MET channels) found at the tips of the hairs.

There is currently a debate in the literature on the relative importance of these two forms of motility in the active amplification process within mammalian hearing; see, for example, Dallos *et al.* (2008). While somatic motility can exert larger forces,

and may hence seem more potent from a mechanical point of view, amplification is also known to occur in lower organisms such as birds and reptiles, whose hair cells do not contain prestin but have rather more pronounced stereocilia. On the other hand, transmission to the basilar membrane motion is more straightforward with a somatic motility hypothesis, and the experimental results of Lagarde *et al.* (2009), in mutant mice, suggest that somatic motility alone is sufficient to match wild type behaviour. It has also been suggested that somatic motility may be too slow. However, Frank *et al.* (1999) have recently shown that somatic motility can operate up to very high frequencies - much higher than the highest that are perceived by humans, for example. The main limitation on the speed of somatic motility seems to be the time needed to charge up the capacitance of the OHC's cell body - a process which involves low-pass filtering with a corner frequency of about 1 kHz. However, taking into account the active mechanism of the hair bundle even this filter can be compensated for, see Ó Maoiléidigh & Jülicher (2010). Indeed the model we present in §3 below suggests that from a modelling point of view, the observed behaviour can be best explained by a combination of both bundle- and somatic motility.

There have been many other explanations of the source of the active process in hearing; see for examples Hudspeth *et al.* (2010); Ashmore *et al.* (2010), and references therein. Of particular note is the work of Zweig (1991), who added a complex, but linear feedback term to a simple travelling-wave model of the basilar membrane; the results were found to reproduce the active response of the cochlea well. See also the work of Steele & Lim (1999) and Geisler (1993), who found similar results using a spatial feed-forward term within the travelling-wave equation. A discussion and extension of these results forms the subject of §4 below.

The measurements in Figs. 1 and 4 all concern the motion of the basilar membrane, rather than of hearing itself. The transduction into neural signals occurs within the IHCs. It is widely held that increased basilar membrane motion is transferred into increased stimulation of the IHCs through shearing motion of the tectorial membrane with respect to the reticular laminar. This motion causes displacement of the hairs of the IHCs, which then causes ion channels to open, which in turn causes depolarisation of the IHCs, allowing the connected nerve fibres to fire.

The rest of this paper is organised as follows. First, we present recent progress on mathematical modelling and experimental investigation of hair cell dynamics. Section 2 introduces some recent progress by Tsaneva-Atanasova and Kennedy on mathematical models of the function of developing inner IHCs. The model is validated using electrophysiological recordings reported here for the first time and simulation results are explained with the aid of numerical bifurcation analysis. Section 3 reviews local nonlinear models of active OHC behaviour, within a fixed transverse section of the organ of Corti. We describe a simple model, first proposed in Szalai *et al.* (2011*b*), which is based on a comprehensive model by Ó Maoiléidigh & Jülicher (2010) with the emphasis on the role of somatic motility, transduction current adaptation and nonlinearity that is consistent with the experimental results in Kennedy *et al.* (2005). We also argue that it is not necessary for local models of the OHC dynamics to take the form of the popular "Hopf oscillator" (Eguíluz *et al.*, 2003) to provide results in agreement with experimental data. We then go on, in §4, to discuss how local models (specifically, of the organ of Corti) can be incorporated into a longitudinal cochlear model, which includes fluid coupling as well as coupling through a feed-forward mechanism. Preliminary results are presented

that show how a longitudinally coupled version of the local OHC model can qualitatively reproduce experimentally observed vibration characteristics of the basilar membrane. Finally §5 draws conclusions and suggests avenues for further work.

2. Modelling the development of inner hair cell function

While outer hair cells serve to mechanically pre-amplify the mechanical vibrations (i.e. sound) that reaches the inner ear, inner hair cells are the proper receptor cells of hearing and are connected to the afferent nerves. Sound transduction by IHCs generates a receptor potential which triggers the coordinated release of neurotransmitters onto the ensemble of auditory nerve fibres. The membrane filter properties that define the input-output function of IHCs are dependent on membrane conductance and capacitance (Raybould *et al.*, 2001). In normal hearing, deflection of the hairs of an IHC causes the opening of mechano-electrical transducer ion (MET) channels. This allows a flow of positively charged ions, which depolarises the cell's plasma membrane, and causes the nerve connections at the basal end of the cell to respond. These signals are then sent through nerve pathways to the brain, which makes sense of them as sounds. This process must be performed at exceptional speed in order to encode the complex characteristics of sound such as speech and music. It is therefore important that the excitability of the membrane is carefully controlled to be ready to respond rapidly.

The main control of the membrane potential in an IHC occurs through the action of calcium on the excitability of the hair cells. Calcium is involved in both the mechanotransduction at the cell's apex and neurotransmitter release at base, see e.g. (Johnson & Marcotti, 2008). Thus, regulation of intracellular Ca^{2+} is important for local dynamic fine-tuning of the IHC membrane filter (Raybould *et al.*, 2001). A delicate calcium balance must be maintained in order for hearing to occur, but more insight is required into how this is achieved. An interesting approach to such a problem is to study how calcium also controls the developmental processes within IHCs. Before we are able to hear, the ear must develop the unique sensory properties of the hair cells and form the intricate connections to the brain. It is believed that a key factor in this process is an increase in calcium ions (Ca^{2+}), that is thought to cause neurotransmitters to be released, which in turn helps guide neural connections to form at the basal end of the cell.

During development, IHCs do not respond to sound but instead are capable of firing spontaneous and evoked Ca^{2+} based spikes that disappear close to the onset of hearing, see e.g. Marcotti *et al.* (2003). These spikes generate sufficient Ca^{2+} influx to trigger neurotransmitter release, see e.g. Johnson *et al.* (2005), and activate small conductance Ca^{2+} activated K^+ K_{Ca} currents (so-called SK2 currents) that are known to be expressed in the cochlea, see e.g. Rennie *et al.* (2004). Under basal conditions the membrane potential of these cells is constant near its equilibrium value and the intracellular calcium concentration, $[Ca^{2+}]_i$ is low, so the K_{Ca} channels are closed. The negative membrane potential keeps the voltage-dependent Ca^{2+} channels and $[Ca^{2+}]_i$ low, and no significant neurotransmitter release takes place. Upon stimulation, which generally leads to depolarisation, the membrane potential increases, opening voltage-gated Ca^{2+} channels. This results in Ca^{2+} influx into the cell cytosol, which stimulates the release of neurotransmitters, see e.g. (Johnson *et al.*, 2007). The increase of $[Ca^{2+}]_i$ opens K_{Ca} channels, generating

outflow of K^+ ions, which repolarises the membrane potential. This repolarisation leads in turn to closure of voltage-gated Ca^{2+} channels and subsequent decrease in the levels of intracellular calcium concentration. In immature IHCs, the combined sequence of events described above triggers repetitive rises (oscillations) in the intracellular calcium concentration that are accompanied by action potential firing in the form of single spikes, as well as plateau-bursting electrical activity (see new data in the right-hand panel of Fig. 2(b), more details of which will be presented elsewhere). Plateau-bursting electrical activity is characterised by periodic switches between an active (depolarised) phase accompanied by increase in $[Ca^{2+}]_i$ and a silent (repolarisation) phase during which $[Ca^{2+}]_i$ decreases.

We have developed a simple preliminary model based on realistic interaction between ion channels to describe how Ca^{2+} influx and buffering generate a $[Ca^{2+}]_i$ signal within developing IHCs. Our model is of Hodgkin & Huxley (1952) type, and is based on the voltage-clamp experimental data obtained from immature IHCs see, e.g., Marcotti *et al.* (2003), Marcotti *et al.* (2004) and (Johnson & Marcotti, 2008). (Further details, including the parameter fitting technique, will be presented elsewhere.) The model equations take the form of four coupled ordinary differential equations (ODEs) for the membrane potential V_m, the concentration of intracellular calcium $c = [Ca^{2+}]_i$, an activation variable n and an inactivation variable h associated with the voltage dependent K^+ channels:

$$C_{\rm m}\frac{dV_{\rm m}}{dt} = I_{\rm app} - I_{\rm Ca} - I_{\rm K} - I_{\rm K_{Ca}} - I_{\rm leak}, \tag{2.1}$$

$$\frac{dn}{dt} = \frac{n_\infty(V_{\rm m}) - n}{\tau_{\rm n}(V_{\rm m})}, \tag{2.2}$$

$$\frac{dh}{dt} = \frac{h_\infty(V_{\rm m}) - h}{\tau_{\rm h}}, \tag{2.3}$$

$$\frac{dc}{dt} = f_{\rm c}\beta\left(-\alpha I_{\rm Ca}(V_{\rm m}) - \frac{k_{\rm PMCA}c^2}{c^2 + K_{\rm p}^2}\right) - k_{\rm SERCA}c + p_{\rm ER}(c_{\rm ER} - c). \tag{2.4}$$

Here, $C_{\rm m}$ is the membrane capacitance, $\tau_{\rm n}(V_{\rm m})$ is the activation time constant for the voltage dependent K^+ channels, $\tau_{\rm h}$ is the inactivation time constant for the voltage dependent K^+ channels, $n_\infty(V_m)$ and $h_\infty(V_m)$ are the steady state functions for n and h, respectively. Equation (2.1) describes the overall dynamics in which the rate of change of membrane potential $V_{\rm m}$ is balanced by the various ionic currents. These currents include the voltage gated calcium current $I_{\rm Ca}$, the voltage gated K^+ current $I_{\rm K}$, and the Ca^{2+}-sensitive potassium current $I_{\rm K_{Ca}}$. Specific forms of the currents included in the model are

$$\begin{aligned} I_{\rm Ca}(V_{\rm m}) &= g_{\rm Ca}m_\infty(V_{\rm m})q_\infty(c)(V_{\rm m} - V_{\rm Ca}),\\ I_{\rm K}(V_{\rm m}, n) &= g_{\rm K}nh(V_{\rm m} - V_{\rm K}),\\ I_{\rm K_{Ca}}(V_{\rm m}, c) &= g_{\rm K_{Ca}}s_\infty(c)(V_{\rm m} - V_{\rm K}),\\ I_{\rm leak}(V_{\rm m}) &= g_{\rm leak}(V_{\rm m} - V_{\rm leak}), \end{aligned}$$

and the steady state activation/inactivation functions are

$$
\begin{aligned}
m_\infty(V_\mathrm{m}) &= \left(1+\mathrm{e}^{(V_{\mathrm{m_L}}-V_\mathrm{m})/s_m}\right)^{-1},\\
n_\infty(V_\mathrm{m}) &= \left(1+\mathrm{e}^{(V_\mathrm{n}-V_\mathrm{m})/s_n}\right)^{-1},\\
\tau_\mathrm{n}(V_\mathrm{m}) &= 0.0022+0.0029\,\mathrm{e}^{-V_\mathrm{m}/14.3},\\
h_\infty(V_\mathrm{m}) &= 0.214+0.355\left(1+\mathrm{e}^{(V_\mathrm{m}-V_\mathrm{h1})/s_{h1}}\right)^{-1}+0.448\left(1+\mathrm{e}^{(V_\mathrm{m}-V_\mathrm{h2})/s_{h2}}\right)^{-1},\\
q_\infty(c) &= \left(1+\frac{c}{K_q}\right)^{-1},\\
s_\infty(c) &= \frac{c^4}{c^4+k_\mathrm{s}^4},
\end{aligned}
$$

where $q_\infty(c)$ is the steady state Ca^{2+}-dependent inactivation of the voltage gated calcium current (Grant & Fuchs, 2008) and $s_\infty(c)$ is the steady state Ca^{2+}-dependent activation of the K_{Ca} channels.

The plateau spikes during a burst are due to the interaction between the voltage-dependent calcium and potassium currents I_{Ca} and I_K. There is also a slow process included, which is responsible for the shifts between the active and the silent phases. The slow modulation is provided by the intracellular calcium concentration c, which is a negative feedback variable. The rate of change of c is also given by a balance equation (2.4) for the fluxes involved in its dynamics. The Ca^{2+} flux across the plasma membrane is given by the difference between the Ca^{2+} influx, represented by the voltage-gated calcium current, and Ca^{2+} efflux through the plasma membrane Ca^{2+} pump. Here, $C_\mathrm{m}=10^{-5}\times A_\mathrm{cell}$ is the membrane capacitance, and f_c is the fraction of free to total cytosolic Ca^{2+}, $\alpha=10^5/(2\times 9.65\times A_\mathrm{cell})$ is a factor that converts current to flux, $A_\mathrm{cell}=\pi\times d_\mathrm{cell}^2$ is the area of the cell, and k_PMCA is the plasma membrane Ca^{2+} ATPase pump rate. Since c represents the free Ca^{2+} concentration in the cytosol, the corresponding fluxes are multiplied by the fraction of free to total cytosolic calcium, f_c.

The values of all parameters used in the model simulations are as follows: k_PMCA = 3.6s^{-1}, I_app = 0pA, k_SERCA = 1.2s^{-1}, K_p = 0.08μM, d_cell = 15μm, k_s = 1.25nS, V_K = $-$60mV, g_Ca = 2.4nS, V_Ca = 60mV, g_K = 2.85nS, V_leak = $-$20mV, g_leak = 0.12nS, $V_{\mathrm{m_L}}$ = $-$26.7mV, V_n = $-$16mV, s_m = 11.5mV, s_n = 10mV, V_h1 = $-$60.5mV, V_h2 = $-$17.8mV, s_{h1} = 6.8mV, s_{h2} = 7.1 mV, k_q = 0.6μM, τ_h = 0.55s^{-1}, $[Ca^{2+}]_\mathrm{ER}$= 500μM, f_c = 0.01.

It has been established experimentally that the activation of K_{Ca} channels controls the magnitude and duration of IHCs response to stimulation (Marcotti *et al.*, 2004). Figure 2(a) presents a validation of our IHC model, illustrated via simulations of a gradual reduction in the amount of $I_{K_{Ca}}$, achieved by reducing the maximum channel conductance $g_{K_{Ca}}$in the model. These simulations accurately reproduce previously published experimental data of continuous recordings of voltage responses in the presence of K_{Ca} channel blocker (see e.g. Fig. 3C in Marcotti *et al.* (2004)). As K_{Ca} channel activity is decreased in the model, spike repolarisation gradually slows and eventually begins to fail leading to prolonged depolarisations. Moreover the model predicts that, in response to spikes, signals of intracellular calcium c initially rise sharply and are brief. However as repolarisation begins to fail the resting

c-value rises and the c-increases are less sharp, rising throughout depolarisation. Interestingly, our experimental recordings of spikes (top traces in the right panel of Fig. 2), and their corresponding near membrane c-signals (bottom), confirm that during prolonged action potentials (bursts) c-signals appear larger in magnitude and duration. This would presumably result in increased neurotransmitter release probability (Johnson *et al.*, 2007). In the left-hand panel of Fig. 2(b) we show typical IHC model solutions for a fixed value of $g_{\mathrm{K_{Ca}}} = 4$ nS. These results show that our model supports periodic solutions of mixed type, that are composed of a single spike and a burst with several small amplitude spikes. We have also observed such patterns of electrical activity in immature IHC as shown in the right-hand panel of Fig. 2(b).

In order to gain an insight into the effect of changing maximum $\mathrm{K_{Ca}}$ channel conductance, $g_{\mathrm{K_{Ca}}}$, we have performed a bifurcation analysis of the full model system Eqns. (2.1)-(2.4) using $g_{\mathrm{K_{Ca}}}$ as a bifurcation parameter. Note that $g_{\mathrm{K_{Ca}}}$ also indirectly affects the time scale at which c changes in the model (Eqn. (2.4)). The corresponding bifurcation diagram of the full IHC model, presented in three dimensional ($g_{\mathrm{K_{Ca}}}$ c, V_{m})-space is shown in Fig. 2(c). The bifurcation diagram of our model shows the emergence of complex bursting from a primordial, large amplitude spiking solution that undergoes a cascade of bifurcations in the full system as the parameter, $g_{\mathrm{K_{Ca}}}$, decreases. For $g_{\mathrm{K_{Ca}}} \approx 9.25$ the branch of periodic orbits that corresponds to stable large amplitude spiking loses stability in a period-doubling bifurcation (PD). As $g_{\mathrm{K_{Ca}}}$ decreases a new stable period-2 orbit emanates from PD and corresponds to a 2-large spikes bursting solution. This period-2 bursting attractor loses stability in another period-doubling bifurcation that gives rise to a complex period-4 bursting solution (not shown) that is stable for considerably smaller range of values of $g_{\mathrm{K_{Ca}}}$ and in turn leads to a classical period-doubling cascade to chaos (not shown). However the range of values for $g_{\mathrm{K_{Ca}}}$ for which this behaviour is found is rather narrow, and we will not focus on it further. Instead, we concentrate on the stable complex bursting behaviour of the IHC model that occurs over a wider range of $g_{\mathrm{K_{Ca}}}$-values.

Direct numerical simulations of Eqns. (2.1)-(2.4) show that decreasing $g_{\mathrm{K_{Ca}}}$ results in complex bursting solutions with more small spikes. Thus we continue such periodic orbits, namely with 1-large spike + 2, 3, 4, 5, 6, or 7 small spikes, in parameter $g_{\mathrm{K_{Ca}}}$. We find that they lie on isolated solution branches, or isolas, as illustrated in Fig. 2(c). As $g_{\mathrm{K_{Ca}}}$ decreases each of these isolas that we compute loses stability in period-doubling bifurcations (not shown) that presumably give rise to period-doubling solutions and generate further complex behaviour that is beyond the scope of this paper. Examples of complex bursting trajectories with 1-large spike + 2, 3, 4, 5, 6, or 7 small spikes are superimposed on the bifurcation diagram in Fig. 2(c). Note also that as $g_{\mathrm{K_{Ca}}}$ decreases, the stable portions of the isolas become smaller, resulting in smaller regions in parameter space where bursts with large number of small spikes exist.

This behaviour can readily be understood from a physiological point of view, since decreasing $g_{\mathrm{K_{Ca}}}$ effectively slows down the calcium component of the bursting orbits in the full system (2.1)-(2.4), hence the trajectory spends more and more time in the direction in the region of phase space with large c and as a result generates more spikes within a burst. Consequently the longer bursts are accompanied by larger $\mathrm{Ca^{2+}}$ signals.

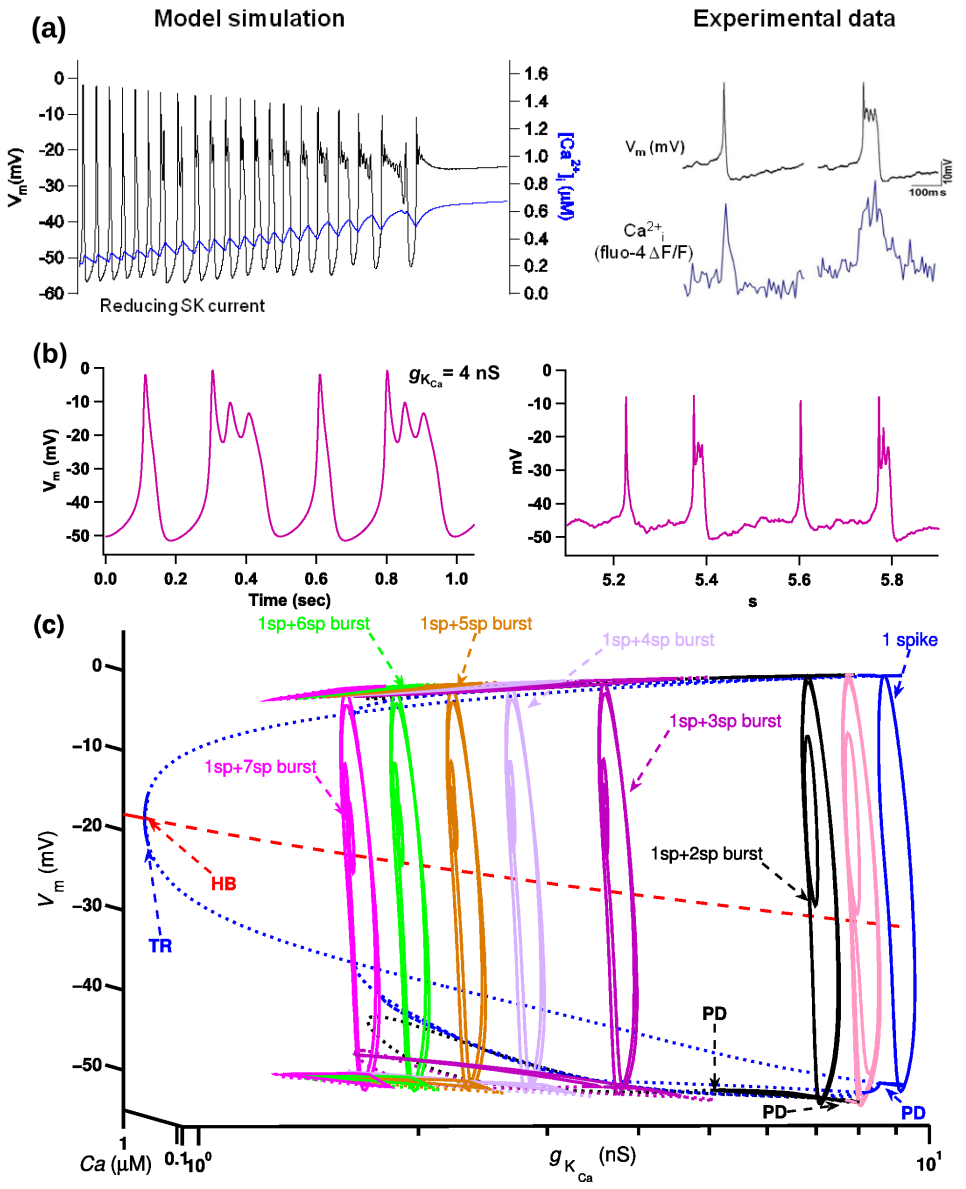

Figure 2. (a) Model simulation and experimental recordings of the effects of blocking SK currents on the frequency and duration of action potentials, and the corresponding whole cell calcium signals. (b) Typical IHC model responses for a fixed value of $g_{\mathrm{K_{Ca}}}$ = 4 nS. (c) Three dimensional bifurcation ($g_{\mathrm{K_{Ca}}}$, c, V_{m}) diagram of the full IHC model; HB-Hopf bifurcation; TR-torus bifurcation; PD-period-doubling bifurcation; broken lines denote unstable solution branches. Sample bursting trajectories with increasing number of spikes, i.e decreasing values of $g_{\mathrm{K_{Ca}}}$ = 9.5; 8.5; 8; 4; 3; 2.5; 2.25; 2 are superimposed on the bifurcation diagram of the full system.

These results on the dynamics of IHCs, while not describing actual hearing, are likely to be important in development since the levels of intracellular calcium

are instrumental for the regulation of neurotransmitter release. More widely, by correctly fitting mathematical models to the more experimentally amenable developing IHCs, we can in principle change parameters to represent mature IHCs in order to understand how they operate within hearing. For example, the transition between various oscillatory regimes could be regarded as a form of plasticity of the intrinsic membrane properties of IHCs, and thus could have a profound effect on their function. The mathematical model described here, carefully validated with new experimental results, will play a key role in developing this understanding.

3. Micro-mechanical models of outer hair cell amplification

While the IHCs are believed to be primarily responsible for encoding acoustic stimuli, the primary role of the OHCs appears to be cochlear amplification (Ashmore *et al.*, 2010). As described in §1, OHCs provide two forms of motility: hair bundle motility (Kennedy *et al.*, 2005) and somatic motility (Brownell *et al.*, 1985).

A schematic of an OHC can be seen in Fig. 3(c). Like the IHC, the OHC has MET (ion) channels that are connected to adjacent hairs in the bundle through elastic fibres, i.e. the tip links. The tip links are presumed, as in non-mammalian hair cells, to be coupled to myosin motors that pre-tense the tip link, perhaps to the most sensitive state of the MET channels. The MET channels are not only mechanically sensitive, but also Ca^{2+} sensitive. This provides a fast adaptation mechanism to tune the operating point of the entire hair bundle (Kennedy *et al.*, 2003). The myosin motors are also Ca^{2+} sensitive; that is, their force decreases with increasing Ca^{2+} concentration.

It has been suggested that the negative stiffness seen in mammalian OHCs, together with spontaneous oscillations of the hair bundle that has been observed in lower vertebrates, e.g., in bullfrog, suggest that the nonlinearity of hair cells can be essentially modelled as that of a nonlinear oscillator undergoing a Hopf bifurcation. (Eguíluz *et al.*, 2003). See Hudspeth (2008) for a detailed review, including appealing evidence that a forced Hopf bifurcation normal form can give rise to a compressive nonlinearity and a possible explanation for otoacoustic emissions and two-tone interference in hearing (Jülicher *et al.*, 2001).

In order to understand the possible physiological basis for the Hopf bifurcation hypothesis, Tinevez *et al.* (2007) adapted a model of the myosin motor mechanism constructed by Assad & Corey (1992) that can account for gating currents observed on a voltage clamped cell, as well as the mechanical properties of the hair bundle in bullfrogs. The current through the ion channels is qualitatively similar to that illustrated in Fig. 3(b). In particular, Tinevez *et al.* (2007) adapted the model to describe mammalian hair bundle dynamics, based on the experimental data of Kennedy *et al.* (2005). It was found that this model can indeed undergo Hopf bifurcation.

Ó Maoiléidigh & Jülicher (2010) incorporated this myosin motor dynamics in their unified ODE model of an OHC which also includes the charge dynamics and linear coupling to all the structural elements in the cochlear cross-section. Recently, Szalai *et al.* (2011*b*) analysed a version of this model and various other simplified ODE models using bifurcation analysis. They find that the dynamics of the system contains many local bifurcations including saddle-node, cusp and Hopf bifurcations of the equilibrium state. They argue that the presence of a bifurcation *per se* is not

the most important feature needed to reproduce the observed compressive nonlinear response; rather it is the form of the nonlinearity that is key.

We present here a simplified model of the dynamics of the organ of Corti that captures what we believe to be the simplest ingredients that are consistent with physiological observations. For more details of how this model may be seen as a reduction of that of Ó Maoiléidigh & Jülicher (2010), see Szalai *et al.* (2011*b*). The model is depicted schematically in Fig. 3(d). The model includes adaptation due to hair bundle displacement and nonlinearity of the transduction current. The actual force to move the basilar membrane is exerted via the OHC's somatic motility mechanism. We assume an elastic and underdamped basilar membrane. The hair cells connect to the basilar membrane through the elastic Deiters' cells on one hand, and are rigidly fixed to the reticular lamina, which provides a stationary frame. The passive organ of Corti mechanism is assumed to stimulate the hair bundle, which in our model does not exert any force.

We use a simplified approach to describe the transduction current I as a function of the hair bundle displacement. To keep a consistent notation with earlier models, in particular the work of Ó Maoiléidigh & Jülicher (2010), we refer to the deflection of the tip link from its equilibrium position via an adaptation variable y_a. Specifically we assume

$$\dot{y}_a = -\kappa(y_a - Z), \tag{3.1}$$

$$I = -P_{\mathrm{O}}(\Delta(\alpha y_a + \beta \dot{y}_a)), \tag{3.2}$$

where Z is the deflection of the hair bundle, and the open probability function P_{O} is given by the Boltzmann function

$$P_{\mathrm{O}}(y) = \frac{1}{1 + \mathrm{e}^{-y}}$$

where the induced current has been scaled to unity if the ion channels are fully open. In contrast to previous work, we do not include separate dynamics for the hair bundle displacement y and the tip link y_a, as this is only a phenomenological description of the data in Kennedy *et al.* (2005). The behaviour of the model is illustrated in Fig. 3(a-b). As in the experiments, we stimulate the hair bundle in the model with step displacements of different magnitude (shown in Fig. 3(a)). This results in peaks of the transduction current whose maximum value depends on the height of the stimulating step with the function P_{O}. When the stimulation is held the current falls to almost zero; that is the adaptation is nearly complete. This means that the transduction current is more of a function of the hair bundle velocity than its position. We found that the values $\alpha = 0.1$ and $\beta = 1$ form a good fit with the experimental observations (see Szalai *et al.* (2011*b*) for more details). The parameter Δ is an overall scale factor of the argument that controls the slope of P_{o} at equilibrium, and can be determined from energetic considerations of the ion channels (Markin & Hudspeth, 1995).

To include (3.1) and (3.2) as a feedback mechanism, we assume that the basilar membrane is modelled as a linear oscillator with natural frequency ω_0, the CF of the longitudinal position in question, and damping ratio ζ. This basilar membrane motion is supposed to be coupled to the OHC through the Deiters' cells, that are again represented by a spring and a damper. We suppose that the spring and

damping constants of this coupling are chosen so that the extension $l(t)$ of the OHC causes an additional force on the basilar membrane equivalent to a reduced restoring force $-f_1\omega_0^2 l$ and reduced damping $-2f_0\zeta\omega_0\dot{l}$.

The extension $l(t)$ of the OHC we suppose to be controlled linearly by somatic motility. Specifically the excess charge q in the hair cell is assumed to leak at rate γ and that the hair cell expands and contracts from its equilibrium length l_0 in direct proportion to the excess charge. For simplicity the units of the charge are chosen so that $l(t) = l_0 + q(t)$. The hair cell is charged by the transduction current. The hair bundle excitation is driven by the basilar membrane motion $z(t)$ and indirectly by the assumed sinusoidal pressure difference $p = F\sin\omega t$. Even though the indirect forcing by the pressure is small, its effect can be rather large due to the sensitivity of the hair bundle. A parameter ϵ is included to represent the relative importance of $p(t)$ on the motion of the basilar membrane z and on the deflection of the hair bundles y_a.

Under the above assumptions, the governing set of equations of the organ of Corti model is

$$\begin{aligned} \ddot{z} &= -2\zeta\omega_0\left(\dot{z} - f_0\dot{q}\right) - \omega_0^2\left(z - f_1 q\right) + \epsilon F\sin\omega t, \\ \dot{y}_a &= -\kappa\left(y_a - \left(z + F\sin\omega t\right)\right), \\ \dot{q} &= -\gamma q + P_{\mathrm{O}}(\Delta(\alpha y_a + \beta\dot{y}_a)) - P_{\mathrm{O}}(0). \end{aligned} \tag{3.3}$$

Note that the only nonlinearity is the open probability function P_{O}.

The bifurcation diagram of (3.3) can be seen in Fig. 3(e). The white region is stable and bounded by a pitchfork bifurcation (horizontal line) and a Hopf bifurcation curve (diagonal line). Both bifurcations are supercritical, hence there is no additional dynamics of the unforced system in the stable region other than the equilibrium. We have found that within the white stability region, the system is rather robust to parameter changes. At our chosen set of parameters (denoted by a cross in Fig. 3(e)) the response of the model can be seen in Fig. 3(f). The response has the desired qualitative feature of being linear for small forcing amplitude, compressive for medium amplitudes and linear again for higher amplitudes. One might notice that its tuning is rather sharp, sharper than is possible by a single degree of freedom (DOF) oscillator, but less sharp than a two DOF oscillator. This is due to the additional dynamics from the adaptation and charging of the hair cell.

One conclusion from these results is that the Hopf bifurcation normal form is too simplistic to describe the physiology. The presence of a Hopf bifurcation within the bifurcation diagram of Fig. 3(e), though, suggests a possible source of otoacoustic emissions as being due to the consequent limit cycle oscillation that might result from a perturbation to the system's parameters away from its stable operating point. It has been suggested that spatial inhomogenity in the cochlea might cause such a perturbation (Elliot *et al.*, 2009). However, the Hopf bifurcation present in this cochlear model, is more like a global than local feature of the cochlea. In particular, we believe that the cochlea is not an ensemble of critically tuned Hopf oscillators, as has been proposed. It is better to think of the cochlea as being a coupled system of simple nonlinear oscillators, which may exhibit a Hopf bifurcation as an emergent feature. In fact, as we outline in the next section, it is the nature of the longitudinal coupling between these oscillators that seems to be the most important feature in explaining experimental observations.

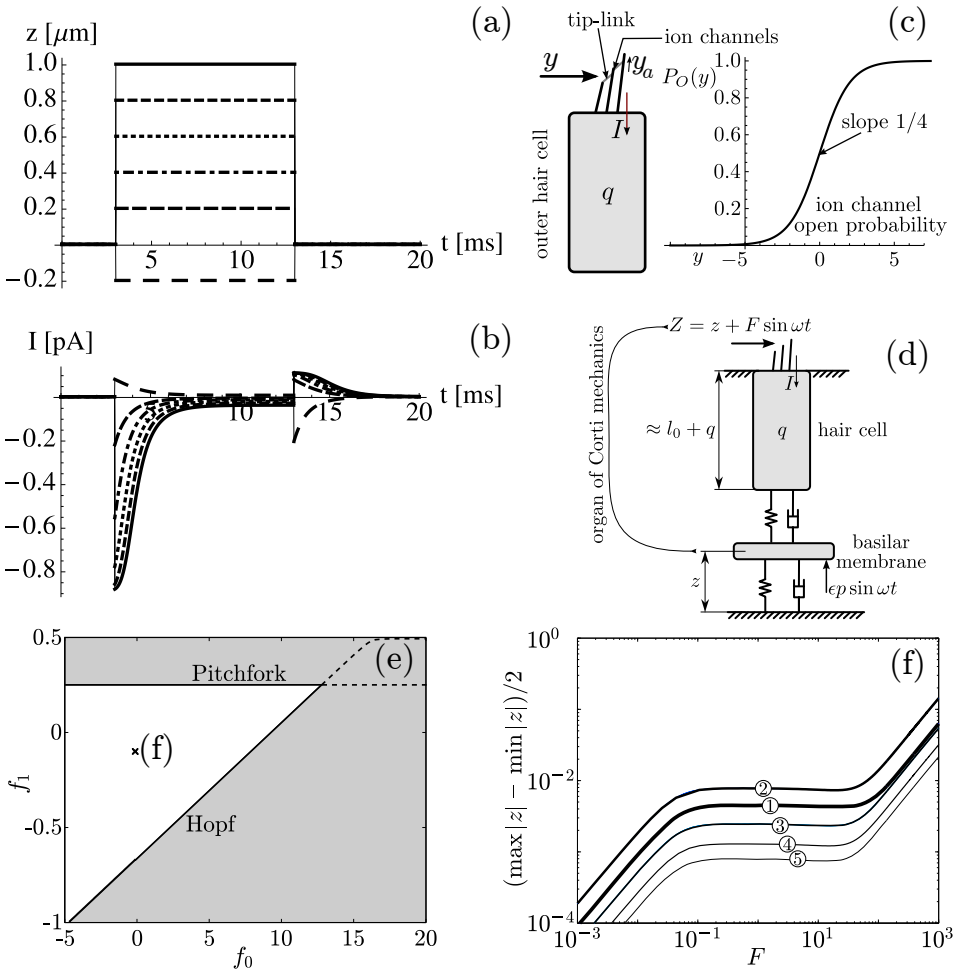

Figure 3. Outer hair cell active mechanisms: (a) applied hair bundle stimulation and (b) the corresponding transduction output current through the ion channels; (c) schematic depiction of the of the hair bundles and the outer hair open probability function; schematic description of the overall mechanics. (e) Bifurcation diagram of the mathematical model (3.3) see text for details and (e) the mechanical response of the model at frequencies: ① 5kHz, ② 6.6kHz, ③ 8kHz, ④ 9kHz and ⑤ 10kHz. Other parameter values used are $\alpha = 0.1$, $\beta = 1$, $\kappa = 6.6$, $f_0 = f_1 = -0.1$, $\omega_0 = 6.6 \times 2\pi$, $\zeta = 0.1$, $\epsilon = \gamma = 1/20$ and $\Delta = 8$.

4. Longitudinal coupling

The organ of Corti model in §3, even though it has some desirable features, is far from complete. The cochlea cannot simply be described as an ensemble of disconnected oscillators each subject to a simple pure-tone input. In truth, there is significant longitudinal coupling between individual organ of Corti cross-sections. Effects that cause this coupling include the longitudinal stiffness of the basilar membrane (which is significantly weaker than its transverse stiffness), the motion of the tectorial membrane, the fluid motion, the fact that the hair cells themselves tilt in the longitudinal direction, and that the Deiters' cells are coupled longitudinally

through their so-called phalangeal processes to the reticular lamina (see Fig. 4(a) for a schematic).

Early models of the cochlea assumed no coupling between basilar membrane cross-sections, other than the fluid motion in the ducts of the cochlea. These models could not account for every detail of the basilar membrane vibration, whether or not they included higher spatial dimensional fluid motion. On the other hand, Zweig (1991) determined the impedance of the basilar membrane necessary to produce observed basilar membrane response. He found that the effective basilar membrane oscillator must have a negative damping coefficient and a linear time-delayed feedback term. Such a model is rather difficult to underpin physiologically. The negative damping could be thought of as a crude model of OHC dynamics, but there is no obvious physiological evidence for a local time-delay of the appropriate duration in the organ of Corti.

The puzzle of Zweig however can be resolved by other means. Steele & Lim (1999) and Geisler (1993) suggested that a longitudinal forward coupling mechanism in the cochlea can produce the same result. Recent work by Szalai *et al.* (2011*a*) provides further evidence in this direction, and an explanation of the similarities and differences between temporal delay and spatial feed-forward. Other forms of longitudinal coupling could arise from a second travelling wave, as suggested by Hubbard (1993), that could be related to either the tunnel of Corti flow (Karavitaki & D.C., 2007), or the waves of the tectorial membrane (Ghaffari *et al.*, 2007). Recently Meaud & Grosh (2010) considered simple plate models for the basilar membrane and the tectorial membrane. They showed that the combined effects of these yield longitudinal coupling that is bidirectional. This bi-directional coupling was found to lead to a cochlear response that has broader, more realistic, peaks as well as to lead to increased stability.

In this paper we use a combination of passive bidirectional coupling and active forward coupling. The bidirectional coupling is inspired by Meaud & Grosh (2010) while the spatial feed-forward coupling is used as more realistic surrogate of the the time delay in Zweig's model (Szalai *et al.*, 2011*a*). We then assume that the micromechanics is described by (3.3) with some simplifications.

Specifically, the model consists of two parts: the fluid dynamics in the chambers of the cochlea, and the micromechanical model of the organ of Corti. As is common in modelling the fluid mechanics, we assume an incompressible and inviscid fluid description of the perilymph, which yields a wave equation for the pressure difference p between the scala tympani and scala vestibuli, and the basilar membrane displacement z,

$$\frac{\partial^2 z}{\partial t^2}(x,t) = \frac{\epsilon^2}{m}\frac{\partial^2 p}{\partial x^2}(x,t). \tag{4.1}$$

Here, the lumped parameter $\epsilon \approx 0.025$ is a function of the geometry of the cochlear chambers and the density of the perilymph fluid, while m is the mass surface density of the basilar membrane. We scale the cochlea length to unity, therefore $0 \leqslant x \leqslant 1$.

To describe the basilar membrane motion we use a simplified version of our local model (3.3). First it is no longer necessary to introduce the applied forcing term $p = \sin(\omega_0 t)$ into the stimulation of the hair cells. Instead, we suppose that the basilar membrane (the main elastic member within the organ of Corti) drives all mechanical components within a cross-section, including the motion between the tectorial membrane and reticular lamina that stimulates the OHC hair bundles.

Hence the variable Z can be replaced with something strictly proportional to the basilar membrane displacement z. Also, we assume that the current adaptation is rather fast compared to the other dynamics, that is, the adaptation variable y_a and the basilar membrane displacement z are also strictly proportional. Without loss of generality, we can assume $y_a = z$. The governing equations are therefore

$$\begin{aligned}\frac{p(x,t)}{m} &= \ddot{z}(x,t) + 2\zeta\omega_0\dot{z}(x,t) + \omega_0^2\left(z(x,t) - f_b q(x-h(x),t)\right)\\ &\quad - \omega_0^2\frac{f_b}{2}\left(z(x-h(x),t) + z(x+h(x),t)\right)\\ \dot{q}(x,t) &= -\gamma q(x,t) + P_{\mathrm{O}}\left(\Delta\left(\alpha z(x,t) + \beta\dot{z}(x,t)\right)\right) - P_{\mathrm{O}}(0).\end{aligned} \tag{4.2}$$

Another simplification to the model (3.3) is that we use only the charge q and not its derivative as the feed-forward term as a modelling convenience. However, we introduce feed-forward and feed-backward terms from the basilar membrane motion. These two terms are equal in magnitude, as they approximate the longitudinal stiffness of basilar membrane, meaning that the membrane is more like an inhomogeneous elastic plate rather than an ensemble of strings, cf. (Meaud & Grosh, 2010). For computational simplicity here we assume that the feed-forward distance $h(x)$ of the action of the hair cells is the same as the longitudinal coupling distance of the basilar membrane (although this assumption can easily be relaxed). A realistic estimate for the magnitude of $h(x)$ can be computed from the length of the hair cells based on the assumption that the geometry of the organ of Corti is self-similar at different positions along the length of the cochlea. Specifically we take $h(x) = 1.2l(x)$, where l is the length of the OHC.

In order to match the experimental data of Rhode (2007), shown in Fig. 4(b),(c), we assume the following mechanics for the basilar membrane: $l(x) = (0.0027 + 0.0027x)$, natural frequency $\omega_0(x) = 2\pi 20.8(e^{-4.8354x} - 0.1455)$, and damping coefficient $\zeta(x) = 0.03(1-e^{-40(1-x)})+0.1e^{-40(1-x)}$. We also include spatial inhomogenity by assuming that the feedback coefficient f_b has a normal random distribution around $\bar{f}_b(x) = 0.08(1 - e^{-40(1-x)})$ with standard deviation $0.01\bar{f}_b(x)$. Other parameters are the same as in (3.3), with the exception of $\gamma = 1$.

We have used a boundary-value problem formulation to solve (4.1) and (4.2). We also assume that the stapes is moved by a harmonic velocity, that is, $u(0,t) = A\sin\omega t$ where u is the fluid velocity of the scala vestibuli. From the 1D fluid flow equation, we find that $\dot{u}(x,t) = -(1/\rho)p'(x,t)$, where ρ is the fluid density. Hence, assuming that the pressure at the cochlear apex vanishes, we find pressure boundary conditions

$$p'(0,t) = -\rho\omega A\cos\omega t, \qquad p(1,t) = 0. \tag{4.3}$$

For the basilar membrane displacement z and charge q, since the response of the cochlea for a single tone excitation is periodic, we prescribe a periodic boundary condition in time

$$z(x,t) = z(x,t+\frac{2\pi}{\omega}), \qquad q(x,t) = q(x,t+\frac{2\pi}{\omega}) \tag{4.4}$$

The numerical method used to solve (4.1) and (4.2) subject to (4.3) and (4.4) is a finite differences discretisation in space and a piecewise-polynomial approximation, so called orthogonal collocation, in time (de Boor & Swartz, 1973). The solution

of the nonlinear equation is propagated with increasing forcing amplitude A using pseudo-arclength continuation (Doedel *et al.*, 1991). Preliminary numerical results

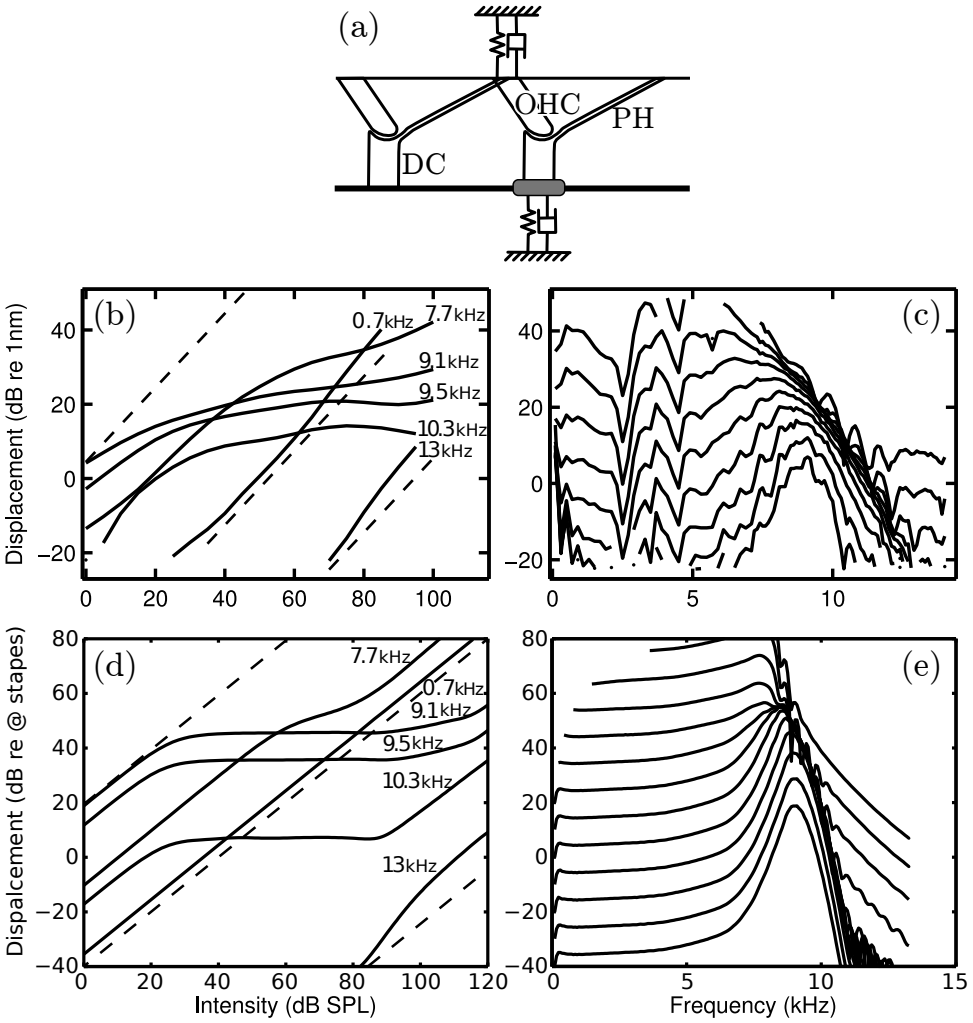

Figure 4. Models with longitudinal coupling. (a) Schematic diagram of the a longitudinal cross-section of the organ of Corti. (b),(c) Experimental data due to (Rhode, 2007) showing I/O functions measured on a chinchilla basilar membrane at CF= 9.1kHz as a function of input amplitude and input frequency. The dashed lines have slope 1 for comparison. Reproduced with permission from ASA. (d),(e) Model predictions of (b) and (c) respectively. See text for details.

are shown in Fig. 4(d-e). More details will be presented elsewhere.

Figure 4 (b-c) shows, for comparison, experimental results from Rhode (2007) at 9.1 kHz characteristic frequency (CF). Figure 4(b) shows the input-output functions for different stimulus frequencies. For frequencies substantially lower than CF the response is linear. For frequencies closer to CF the response becomes com-

pressive for mid range amplitudes and tends towards linear for high amplitudes. The compressive nature remains for very high frequencies but the linear region for higher amplitudes starts earlier. In Fig. 4(c) the cochlear response is shown as a function of frequency at constant amplitudes. For low amplitudes, the response has a distinct broad peak at the CF. With increasing amplitude the peak gets less pronounced and slightly moves towards lower frequencies. The amplitude independent variation at lower frequencies observed in experiments could be due to the middle ear, while wiggles at higher than CF frequencies might be explained by interference of vibrations from the travelling wave and a faster wave (Olson, 1998). Another observation is that in Fig. 4(c) the response at 13 kHz is nearly linear, even a little expansive. This might also be explained by a second sound source perhaps from the compressive wave or the basilar membrane longitudinally coupled dynamics.

In comparison, our model (4.1) and (4.2) yields similar results in Figs. 4(d-e). The significant differences are that the numerical results show sharper responses, which yield somewhat thinner peaks in Fig. 4(e), and curves that are somewhat further apart in Fig. 4(d). Because we do not model the middle ear, amplitude disturbances due to it (at low frequencies) are absent in Fig. 4(e). However, surprisingly the disturbances at high frequencies are reproduced in Fig. 4(e). This is especially striking since the model does not include fast compression waves or any other source that the travelling wave could interfere with. A control simulation with longitudinally smooth feedback $f_b = \bar{f}_b$ shows identical dips in the tuning curves, hence the inhomogeneity of parameters is similarly ruled out as a possible cause. Also, surprisingly, in Fig. 4(d) for the 13 kHz curve we get a similar response to the experimental result. Our speculation is that the early linearity of high frequency input-output functions is due to the longitudinal coupling, without which the curve would be flat up until high-amplitude forcing. The exact mechanism for this linearity however is still under investigation.

5. Conclusions

This paper has reviewed the dynamical properties of the mammalian cochlea, and presented some preliminary results on modelling its specific nonlinear components.

First, we presented a new model, supported by new data, of how inner hair cell calcium currents might play a role in the development of hearing. IHCs Ca^{2+} signalling pathways are thought to be critical to both the intrinsic development of IHCs and the auditory system as a whole. Understanding the basic elements of these signalling pathways in the healthy ear is essential in order to approach future strategies for hair cell regeneration or replacement therapies that may be used to treat conditions such as age related hearing loss. Such understanding could be greatly facilitated by using complementary approaches of experimentation and mathematical modelling.

Next, we reviewed the dynamics of the outer hair cells, which are believed to be the source of cochlear amplification. The nonlinearity of these cells appears to play a significant role in cochlear function, leading to compressive nonlinearity in the basilar membrane response and in sound perception more generally. Based on our synthesis of earlier micromechanical models we introduced a longitudinally coupled cochlear model that includes many aspects of the cochlear mechanism already identified by others. In particular we argue that it is the combination of spatial

feed-forward, longitudinal coupling, somatic motility and nonlinear MET channel open probabilities, that enables our model to agree qualitatively and quantitatively with data.

Note that all of this agreement is found by physiological modelling without assuming *a priori* that the hair bundles are tuned to undergo a local bifurcation. This finding seems to run counter to some current opinion in the literature which suggests the normal form for a Hopf bifurcation is a suitable local model for the mammalian cochlea (see e.g. Hudspeth *et al.* (2010) for a recent opinion piece). Indeed, proponents of a Hopf bifurcation theory point to a supposed 1/3-power law in the amplification data (which does not seem to be universal). In fact it can be shown by harmonic balance (Szalai *et al.*, 2011*b*) that a 1/3-power law comes from the presence of the lowest-order term nonlinear term in any nonlinear function.

One key question that remains, then, is what is the true source of the nonlinearity in the OHC dynamics? Here, we have assumed an open probability function that depends on a mixture of the displacement and rate of displacement of the hair bundles. This provides a good agreement with the experimental data, but does not shed light on the biochemical processes that might cause such a response. This is where future work that incorporates ion-channel modelling as we described for the IHCs might be helpful. In particular, Verpy *et al.* (2008) have found that stereocilin deficient mice lack signatures of nonlinearity, but preserve amplification and sharp tuning that progressively vanishes. Determining the effect of stereocilia links on mechanoelectrical transduction is therefore another avenue to pursue.

One key mathematical technique we have used in this paper and seems especially important when investigating nonlinear models is the use of numerical bifurcation analysis. This method can be useful to test for robustness of mechanisms, to point to possible multistability or plasticity and the proximity of instability. Bifurcation analysis works best on simplified models which capture the essential features believed to be at work.

More generally though, as the nature of the cochlear amplifier is still debated, we need to use more comprehensive simulation models that incorporate the true geometry of the cochlea in order to decide what modelling assumptions play essential roles. Even though linear, the model of Grosh and Meaude described in Ashmore *et al.* (2010) comes closest to this requirement. Careful parametrisation of such models remains a major issue, as does the correct treatment of noise, inhomogenity and within-species heterogeneity.

References

Ashmore, J., Avan, P., Brownell, W. E., Dallos, P., Dierkes, K., Fettiplace, R., Grosh, K., Hackney, C. M., Hudspeth, A. J. *et al.* 2010 The remarkable cochlear amplifier. *Hearing Res.*, **266**(1-2), 1–17.

Assad, J. A. & Corey, D. P. 1992 An active motor model for adaptation by vertebrate hair cells. *J. Neurosci.*, **12**, 3291–3309.

Békésy, G. 1960 *Experiments in hearing.* McGraw Hill.

Brownell, W. E., Bader, C. R., Bertrand, D. & de Ribaupierre, Y. 1985 Evoked mechanical responses of isolated cochlear outer hair cells. *Science*, **227**(4683), 194–196.

Dallos, P. 2008 Cochlear amplification, outer hair cells and prestin. *Curr. Opin. Neurobiol.*, **18**, 370–376.

Dallos, P., Wu, X., Cheatham, M. A., Gao, J., J. Zheng, C. T. A., Jia, S., Wang, X., Cheng, W. H. Y., S. Sengupta, D. Z. Z. H. *et al.* 2008 Prestin-based outer hair cell motility is necessary for mammalian cochlear amplification. *Neuron*, **58**(3), 333 –339.

de Boor, C. & Swartz, B. 1973 Collocation at Gaussian points. *SIAM J. Numer. Anal.*, **10**, 582–606.

Doedel, E. J., Keller, H. B. & Kernévez, J. P. 1991 Numerical analysis and control of bifurcation problems, part II: Bifurcation in infinite dimensions. *Int. J. Bifurcat. Chaos*, **1**(4), 745–772.

Eguíluz, V. M., Ospeck, M., Choe, Y., Hudspeth, A. J. & Magnasco, M. O. 2003 Essential nonlinearities in hearing. *Phys. Rev. Lett.*, **84**(22), 5232–5235.

Elliot, S., Ku, E. & Linton, B. 2009 Time domain model of a nonlinear inhomogeneous cochlea. In *Concepts and challenges in the biophysics of hearing* (eds N. Cooper & D. Kemp), pp. 74–81. 10th International Workshop on the Mechanics of Hearing, Keele 2008: World Scientific.

Frank, G., Hemmert, W. & Gummer, A. W. 1999 Limiting dynamics of high-frequency electromechanical transduction of outer hair cells. *Proc. Natl. Acad. Sci. USA*, **96**, 4420–4425.

Geisler, C. 1993 A realizable cochlear model using feedback from motile outer hair cells. *Hear. Res.*, **68**, 253–262.

Ghaffari, R., Aranyosi, A. J. & Freeman, D. M. 2007 Longitudinally propagating traveling waves of the mammalian tectorial membrane. *Proc. Natl. Acad. Sci. USA*, **104**(42), 16 510–16 515.

Gitter, A. H. 1990 Eine kurze Geschichte der Hörforschung. I. Antike. *Laryngo-Rhino-Otol.*, **69**, 442–445.

Grant, L. & Fuchs, P. 2008 Calcium- and calmodulin-dependent inactivation of calcium channels in inner hair cells of the rat cochlea. *J. Neurophysiol*, **99**(5), 2183–2193. (doi:10.1152/jn.01174.2007)

Helmholtz, H. 1863 *On the sensation of tone.* Dover Publications.

Hensen, V. 1863 Zur morphologie der schnecke des menschen und der zur morphologie der schnecke des menschen und der saugetiere. *Zeits. wiss. Zool.*, **13**(481–512).

Hodgkin, A. L. & Huxley, A. F. 1952 A quantitative description of membrane current and its application to conduction and excitation in nerve. *J. Physiol*, **117**(4), 500–544.

Hubbard, A. 1993 A traveling-wave amplifier model of the cochlea. *Science*, **259**(5091), 68–71.

Hudspeth, A., Martin, P. & Jülicher, F. 2010 A critique of the critical cochlea: Hopf — a bifurcation — is better than none. *J. Neurophysiol.*, **104**(3), 1219–1229.

Hudspeth, A. J. 2008 Making an effort to listen: mechanical amplification in the ear. *Neuron*, **59**, 503–545.

Johnson, S., Adelman, J. & Marcotti, W. 2007 Genetic deletion of SK2 channels in mouse inner hair cells prevents the developmental linearization in the Ca^{2+}dependence of exocytosis. *J. Physiol*, **583**(Pt 2), 631–646. (doi: 10.1113/jphysiol.2007.136630)

Johnson, S. L. & Marcotti, W. 2008 Biophysical properties of CaV1.3 calcium channels in gerbil inner hair cells. *J. Physiol*, **586**(4), 1029–1042. (doi: 10.1113/jphysiol.2007.145219)

Johnson, S. L., Marcotti, W. & Kros, C. J. 2005 Increase in efficiency and reduction in Ca^{2+}dependence of exocytosis during development of mouse inner hair cells. *J. Physiol.*, **563**(Pt 1), 177–191. (doi:10.1113/jphysiol.2004.074740)

Johnstone, B. M. & Boyle, A. J. F. 1967 Basilar membrane vibration examined with the Mössbauer technique. *Science*, **158**, 389–390.

Jülicher, F., Andor, D. & Duke, T. 2001 Physical basis of two-tone interference in hearing. *Proc. Natl. Acad. Sci. USA*, **98**(16), 9080–9085.

Karavitaki, K. & D.C., M. 2007 Evidence for outer hair cell driven oscillatory fluid flow in the tunnel of Corti. *Biophys. J.*, **92**(9), 3284–3293.

Kemp, D. T. 1978 Stimulated acoustic emissions from within the human auditory system. *J. Acoust. Soc. Am.*, **64**, 1386–1391.

Kennedy, H., Crawford, A. & Fettiplace, R. 2005 Force generation by mammalian hair bundles supports a role in cochlear amplification. *Nature*, **443**, 880–883.

Kennedy, H., Evans, M., Crawford, A. & Fettiplace, R. 2003 Fast adaptation of mechanoelectrical transducer channels in mammalian cochlear hair cells. *Nat. Neurosci.*, **6**(8), 832–836. (doi:10.1038/nn1089)

Lagarde, M. M. M., Drexl, M., Lukashkina, V. A., Lukashkin, A. N. & Russell, I. J. 2009 Determining the identity of the cochlear amplifier: electrical stimulation of the tecta mouse cochlea. In *Concepts and challenges in the biophysics of hearing* (eds N. P. Cooper & D. T. Kemp), pp. 106–112.

Lesser, M. B. & Berkley, D. A. 1972 Fluid mechanics of the cochlea I. *J. Fluid Mech.*, **51**, 497–512.

Lighthill, J. 1981 Energy-flow in the cochlea. *J. Fluid Mech.*, **106**, 149–213.

Marcotti, W., Johnson, S. L. & Kros, C. J. 2004 A transiently expressed SK current sustains and modulates action potential activity in immature mouse inner hair cells. *J. Physiol.*, **560**(Pt 3), 691–708. (doi:10.1113/jphysiol.2004.072868)

Marcotti, W., Johnson, S. L., Rusch, A. & Kros, C. J. 2003 Sodium and calcium currents shape action potentials in immature mouse inner hair cells. *J. Physiol.*, **552**(Pt 3), 743–761. (doi:10.1113/jphysiol.2003.043612)

Markin, V. S. & Hudspeth, A. J. 1995 Gating-spring models of mechanoelectrical transduction by hair-cells of the internal ear. *Annu. Rev. Bioph. Biom.*, **24**, 59–83.

Meaud, J. & Grosh, K. 2010 The effect of tectorial membrane and basilar membrane longitudinal coupling in cochlear mechanics. *J. Acoust. Soc. Am.*, **127**(3), 1411–1421.

Olson, E. S. 1998 Observing middle and inner ear mechanics with novel intracochlear pressure sensors. *J. Acoust. Soc. Am.*, **103**(6), 3445–3463.

Ó Maoiléidigh, D. & Jülicher, F. 2010 The interplay between active hair bundle motility and electromotility in the cochlea. *J. Acoustic. Soc. Amer.*, **104**, 1219–1229.

Raybould, N. P., Jagger, D. J. & Housley, G. D. 2001 Positional analysis of guinea pig inner hair cell membrane conductances: implications for regulation of the membrane filter. *J. Assoc. Res. Otolaryngol.*, **2**(4), 362–376.

Rennie, K. J., Manning, K. C. & Ricci, A. J. 2004 Mechano-electrical transduction in the turtle utricle. *Biomed. Sci. Instrum.*, **40**, 441–446.

Rhode, W. S. 1971 Observations of the vibration of the basilar membrane in squirrel monkeys using the mössbauer technique. *J. Acoust. Soc. Am.*, **49**, 1218–1231.

Rhode, W. S. 2007 Basilar membrane mechanics in the 6-9khz region of sensitive chinchilla cocheae. *J. Acoust. Soc. Am.*, **121**(5), 2805–2818.

Robles, L. & Ruggero, M. A. 2001 Mechanics of the mammalian cochlea. *Physiol. Rev.*, **81**(3), 1305–52.

Sellick, P. M., Patuzzi, R. B. & Johnstone, B. M. 1982 Measurement of basilar membrane motion in the guinea pig using the Mössbauer technique. *J. Acoust. Soc. Am.*, **72**, 131–141.

Steele, C. R. & Lim, K. M. 1999 Cochlear model with three-dimensional fluid, inner sulcus and feed-forward mechanism. *Audiol. Neurootol.*, **4**(3-4), 197–203.

Szalai, R., Epp, B., Champneys, A. R. & Homer, M. 2011*a* On time-delayed and feed-forward transmission line models of the cochlea. *J. Mech. Mat. Struct.* In press.

Szalai, R., Ó Maoiléidigh, D., Kennedy, H., Cooper, N. & Homer, M. 2011*b* On the origins of the compressive cochlear nonlinearity. Preprint, University of Bristol.

Tinevez, J., Jülicher, F. & Martin, P. 2007 Unifying the various incarnations of active hair-bundle motility by the vertebrate hair cell. *Biophys. J.*, **93**(11), 4053–4067.

Verpy, E., Weil, D., Leibovici, M., Goodyear, R. J., Hamard, G., Houdon, C., Lefèvre, G. M., Hardelin, J., Richardson, G. P. *et al.* 2008 Stereocilin-deficient mice reveal the origin of cochlear waveform distortions. *Nature*, **456**, 255—258.

Zheng, J., Shen, W., He, D. Z. Z., Long, K. B., Madison, L. D. & Dallos, P. 2000 Prestin is the motor protein of cochlear outer hair cells. *Nature*, **405**(149-155).

Zweig, G. 1991 Finding the impedance of the organ of Corti. *J. Acoust. Soc. Am.*, **89**, 1229–1254.

Zwislocki, J. J. 1948 Theorie der Schneckenmechanik: Qualitative und Quantitative Analyse [Theory of the mechanics of the cochlea]. *Acta Oto-Laryngol.*, **72**, 1–76.